Direct Numeric Simulation of Sheared Convective Boundary Layer Mixing and Entrainment

N. J. Stewart[1], D. W. Holmes[1] and W. Lin[1]

[1]College of Science, Technology & Engineering
James Cook University, Townsville, QLD 4811, Australia

Abstract

Sheared convective boundary layer (SCBL) is a frequently observed boundary layer in nature and industry, with the atmosphere being a common natural case. Due to the combination of interacting turbulent effects in a SCBL, mixing and entrainment is not well understood. In this paper, DNS simulations were performed on a system where stably and unstably stratified shear layers are subjected to the additional effects of an evenly distributed constant heat flux at the bottom boundary. The code used to simulate this system was developed in house, and is implemented using the CUDA programming language for graphical processing units. It implements the incompressible Navier-Stokes equations with the Boussinesq approximation for buoyancy driven flows using a finite difference form of the Semi-Implicit Method for Pressure Linked Equations (SIMPLE).

Introduction

Sheared convective boundary layers are turbulent boundary layers that are prevalent in environmental (in the atmosphere) and engineered systems (such as air conditioning systems). Mixing in SCBLs is driven by three primary sources; convective plumes generated at the lower boundary, shear forces acting at the lower boundary and a shear layer acting above the bottom surface. In the case of the atmospheric boundary layer, there can also be a radiative heat exchange at the upper boundary and phase changes occurring in the cloud layer. SCBLs are capped by a layer of stratified fluid known as the entrainment zone.

Currently the flow behaviour of SCBLs is not well understood and accurate parameterization of entrainment and other flow characteristics is limited [3]. Parameterization used in large scale atmospheric simulations is usually simplified and not necessarily accurate [1]. Characterization of entrainment in the atmospheric boundary layer is essential for problems such as weather prediction and pollution dispersion. Field scale testing of SCBL systems has been limited by the difficulty in taking measurements and isolation of competing processes. Laboratory scale models and numerical modelling have been the focus of improving the understanding of SCBLs.

In this paper we present a form of SCBL where a stratified shear layer with a stationary lower layer is also subjected to a positive flux at the lower boundary. This system is numerically modeled and parameters such as turbulent kinetic energy and turbulent buoyancy flux are investigated.

Numerical Model

Governing Equations and Parameters

To model the SCBL system, the following Navier-Stokes and energy equations need to be solved numerically in 2D,

$$\nabla \cdot \vec{u} = 0, \tag{1}$$

$$\frac{\partial \vec{u}}{\partial t} + \vec{u} \cdot \nabla \vec{u} = -\frac{1}{\rho} \nabla P + \nu \nabla^2 \vec{u} - \beta(T - T_0)\vec{g}, \tag{2}$$

$$\frac{\partial T}{\partial t} + \vec{u} \cdot \nabla T = \sigma \nabla^2 T, \tag{3}$$

where $\vec{u}$ is the velocity vector, t is time, ρ is the density, P is the pressure, ν is the kinematic viscosity, $\vec{g}$ is the gravity vector, β is the coefficient of thermal expansion, T is the temperature, T_0 is the reference temperature and σ is the thermal diffusivity. The Boussinesq approximation is also assumed through the modified gravity term $\beta(T - T_0)\vec{g}$. The components of the velocity vector are written as u and v, which represent the velocity in the x and y directions as shown in figure 1.

The SCBL flow can be characterised by the following dimensionless parameters; the bulk Reynolds number Re_b, the shear Richardson number Ri_s and the flux Rayleigh number Ra,

$$Re_b = \frac{\Delta u h_i}{\nu}, \quad Ri_s = \frac{g \Delta \rho d_0}{\rho_0 \Delta u^2}, \quad Ra = \frac{B_s h_i^4}{\nu \sigma^2}, \tag{4}$$

where Δu is the velocity difference over the shear layer, h_i is the height of the interface, ν is the kinematic viscosity, $\Delta \rho$ is the buoyancy jump over the interface, d_0 is the thickness of the interface, ρ_0 is the reference density and B_s is the flux added at the bottom surface. Some of these parameters are illustrated in figure 1 where the domain setup for SCBL cases is sketched.

Numerical Method

The Semi-Implicit Method for Pressure Linked Equations (SIMPLE) algorithm [2] was implemented in the CUDA programming language and used to solve the SCBL systems. It implements 2nd order discretization schemes for the advection and diffusion terms and is 1st order accurate in time using finite difference methods. The code was previously verified against common test cases for buoyancy driven flows [7]. Direct numerical simulations are run as turbulence models have been shown to be inadequate for the stably stratified entrainment zone [6, 4].

Initial and Boundary Conditions

The initial horizontal velocity and density profiles are shown in figure 1, with the profiles being modified slightly from Smyth and Winters [5] to give the stationary lower layer. The profiles take the form,

$$u(y) = \frac{\Delta u}{2}[1 + \tanh \frac{2}{d_0}(y - h_i)], \tag{5}$$

$$\rho(y) = \frac{\Delta \rho}{2}[1 - \tanh \frac{2}{d_0}(y - h_i)]. \tag{6}$$

The lower boundary is defined as a non slip wall with a Neumann boundary to give a constant flux at the lower surface. The upper boundary is a slipping wall with a zero flux condition. Boundaries on the left and right of the domain are cyclic to impose an infinite field. The properties of the fluid mimic water at $20°C$.

The domain is two dimensional and has a uniform spatial discretization, where $\Delta x = \Delta y = 0.001m$ and a mesh of $N_x = 1400$, $N_y = 350$.
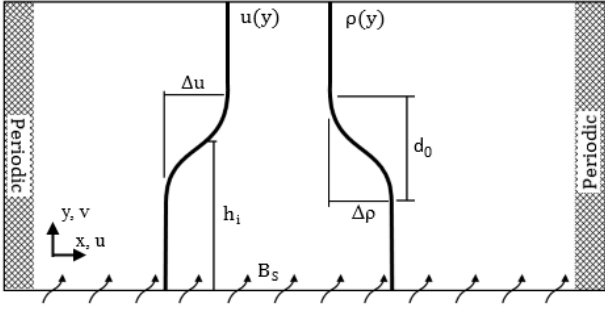
Figure 1. Domain setup of SCBL case and the initial horizontal velocity and density profiles.

Case	Re_s	Ri_s	Ra
1	1750	0.01	0
2	1750	0.01	5×10^{16}
3	1750	0.01	4.5×10^{15}
4	1300	0.02	5×10^{16}
5	850	0.04	5×10^{16}

Table 1. Flow cases.

Test Cases

The cases focused on in this conference paper are listed in table 1. Case 1 is a stratified shear layer without any buoyancy flux. Case 2 is the same shear layer but also subjected to a large buoyancy flux. Case 3 also contains the same shear layer, but with a reduced buoyancy flux. Cases 4 and 5 both have a large buoyancy flux, but reduce the magnitude of the shear layer.

Results and Discussion

Investigating the characteristics of the flow involves inspecting the visual phenomena and then investigating some quantifiable results including the gradient Richardson number, the turbulent kinetic energy, the turbulent buoyancy flux and temperature profiles.

The main interactions that were seen were Kelvin-Helmholtz (KH) instabilities and convective cells. KH instabilities form when shear forces dominate buoyancy forces in a shear layer and are observed as "cat's eye" vortices can be seen towards the middle of case 3 in figure 2. KH instabilities were clear in cases 1 to 3, and were present in the early stages of case 4 but were quickly dissipated thereafter. The convective cells are driven by the added heat flux lowering the density of the region adjacent to the lower boundary. The lower density fluid rises and is eventually capped by the upper layer. Convective cells formed in cases 2 to 5, but were much less dominant in case 3, and are visible in figure 2.

Gradient Richardson Number

Within the field, the stability of the local region can be determined with the local gradient Richardson number, given by

$$Ri_g = \frac{g}{T_0} \frac{\partial T}{\partial y} \left/ \left(\frac{\partial u}{\partial y}\right)^2 \right. . \tag{7}$$

When the gradient Richardson number falls below a critical value (typically $Ri_{g,c} = 0.25$) the shear forces overpower stabilizing buoyancy forces and Kelvin Helmholtz or Holmboe waves form. In cases where the gradient Richardson number is negative, there is a static instability where a higher density fluid is vertically above a lower density fluid. The gradient Richardson number is undefined when there is no velocity gradient.
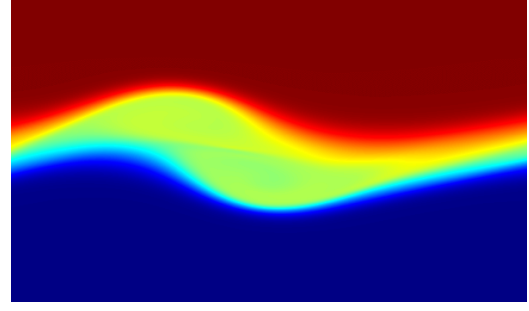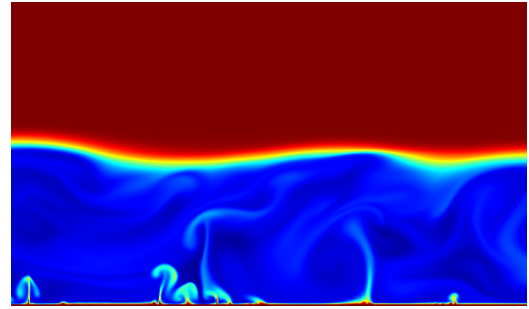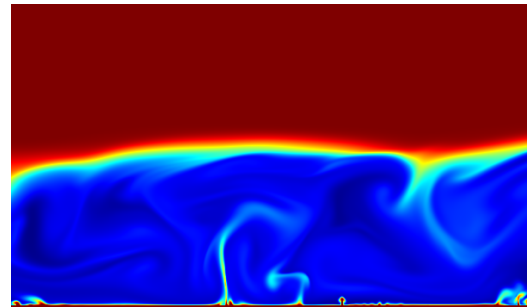

Case 1
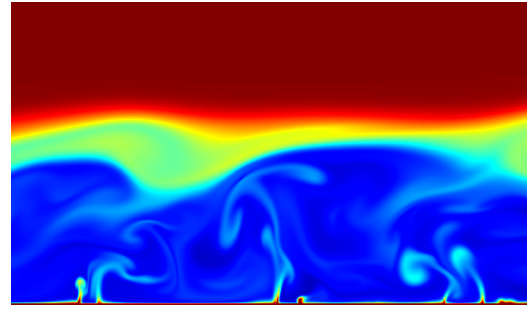
Case 2
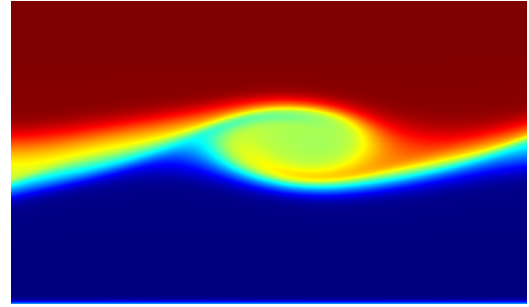
Case 3

Case 4

Case 5

Figure 2. Temperature map of each case at t=40s, truncated to central region, red regions are higher temperature and blue regions are lower temperature.
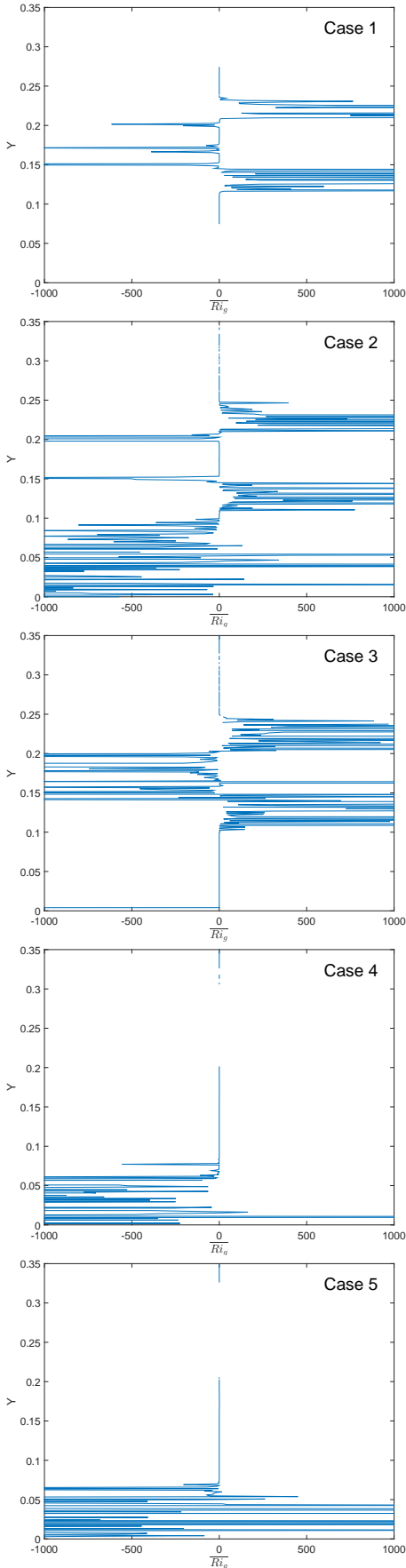
Figure 3. Vertical profiles of the horizontally averaged Ri_g at $t = 20s$.

Figure 3 shows the horizontally averaged gradient Richardson number, $\overline{Ri_g}$, for each case at $t = 20s$. In case 1 (with only the shear layer effect) an unstable mixing region is visible in the entrainment area bounded by the a highly stable region around it, limiting the growth of the KH instabilities. In case 2 a similar form can be seen around the middle shear region. Below this a statically unstable region is present, caused by the added heat flux (which is always unstable). Case 3 shows the same shear layer interaction, but with a significantly reduced instability from the heat flux. Cases 4 and 5 show no shear layer interaction, as by this point of the simulation the flow had stabilized in that region.

Turbulent Kinetic Energy Density

The turbulent kinetic energy (TKE) for the system is the mean kinetic energy per unit mass of the turbulent components of velocity and is given by $\frac{1}{2}\left(\overline{(u')^2} + \overline{(v')^2}\right)$. The TKE is calculated and its time series are presented in Figure 4 for all cases. Case 1 shows a high initial turbulent environment as the KH instabilities form, but as the simulation progresses the growth of these instabilities is limited by the stratification and the total TKE dissipates. Case 2 shows the same system as case 1, but the added flux at the bottom is inherently unstable and causes a continual increase in TKE over the period of the simulation. In this case TKE generation is shown to be dominated by the flux contribution. Case 3 has the same Re_b and Ri_s as the previous two cases, but a lower heat flux. While TKE is always higher than case 1, TKE generation is not as dominant in the later stages of flow, however TKE growth is occurring.

Cases 4 and 5 investigate the effect of varying the shear layer, both cases using the same flux as case 2, but subsequently reduce the velocity difference between the layers. In the middle stages of simulation, TKE density is higher than case 2, and through visual inspection convective plumes can be seen intruding further into the upper region. In the later stages when the lower layer is fully turbulent, TKE density is lower than case 2. From all of the cases it is shown that TKE growth at later stages is heavily dependent on the added heat flux, while earlier stage TKE has a dependence on both the shear layer and the heat flux. The relationship between these effects is of interest and will be investigated further.
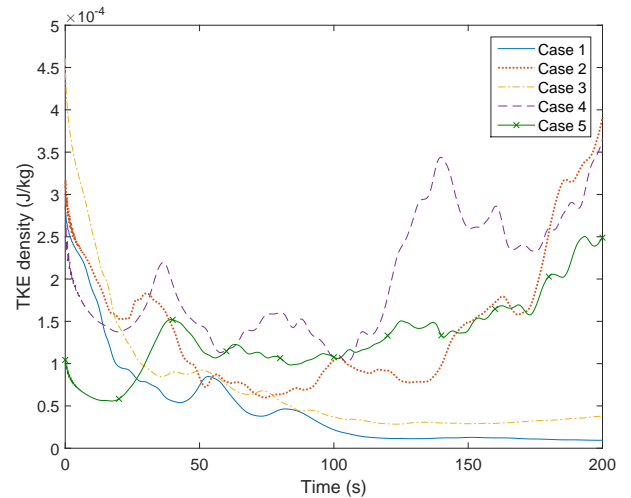

Figure 4. Turbulent Kinetic Energy (TKE) density measured over the duration of the simulation.

Turbulent Buoyancy Flux

To investigate the large increase in TKE density for case 4 at around $t = 140s$ the turbulent buoyancy flux components, given by $\frac{g}{T_0}\overline{v'T'}$, were investigated at that time as shown in figure 5. From this figure it is seen that a largely negative buoyancy flux is occurring within the middle region of flow. When inspecting the density map at that time as shown in the inset of figure 5, a large amount of relatively high density fluid was entrained into the middle region, causing a very unstable configuration. Intrusions into the upper layer are typically dissipated by the bulk flow in the upper layer and with a lower Reynolds number in case 4 the ability for the system to dissipate this intrusion would be reduced, however this interaction is not observed to the same extent in case 5 and warrants further investigation.

During the later stages of flow, as shown in figure 5, the heat flux is the dominant driver of turbulent buoyancy flux for all regions of flow. In case 1 there is very little turbulent buoyancy flux as the flow has stabilized, but in case 2 there is a non-negligible amount of flux in the middle and upper regions.
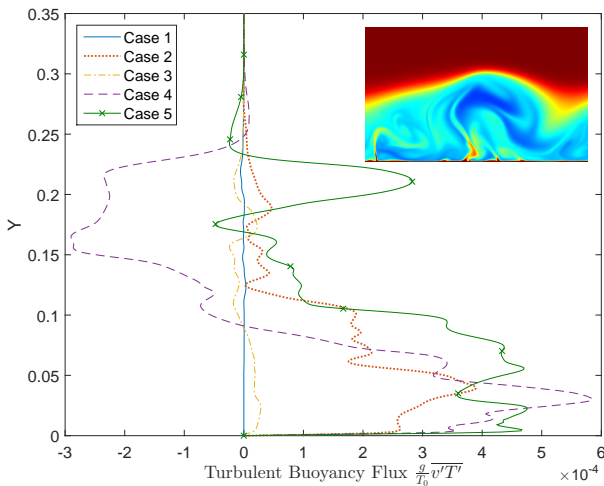

Figure 5. Turbulent component of buoyancy flux horizontally averaged at t=140s. Inset: Temperature structure of case 4 convective cell at t=140s.

Temperature Profiles

When the temperature difference is compared in figure 6, it is possible to see that mixing in the lower layer is dependent mostly on the heat flux added at the lower layer. Case 1 shows a symmetric profile, with the only mixing being caused by the shear layer and the lower region being unmixed outside the shear layer. Cases 2, 4 and 5 had the same heat flux applied and the temperature profiles are similar in the lower region. Case 3 had a profile similar to case 1, but showed an increase in mixing caused by the added heat flux, with a much smaller affect.

Conclusion and Future Work

In this study, the interactions between a stratified shear layer and a constant heat flux were investigated using direct numerical simulations and the flow characteristics were described. The results show that turbulent kinetic energy production and turbulent heat flux are dominated by the added heat flux at later stages, but during formation more complicated interactions are present which need further investigation. From the cases that were analysed, some characteristics of bulk flow were observed but still need to be classified further. Some areas of future inter-
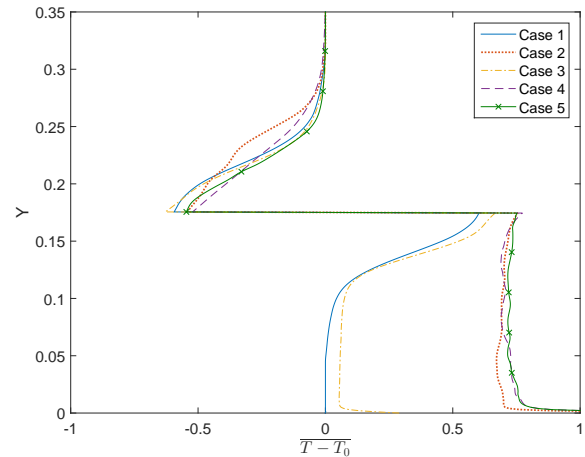

Figure 6. Difference between initial and final (t=200s) horizontally averaged temperature for all cases.

est include; relating late stage TKE generation to heat flux, the affect of the Prandtl number on shear layer and convective cell development, and carrying out 3D simulations to further look at turbulent structures.

Acknowledgements

References

[1] Ayotte, K.W., Sullivan, P.P., Andrn, A., Doney, S.C., Holtslag, A.A., Large, W.G., and Wyngaard, J.C., An Evauluation of Neutral and Convective Planetary Boundary-Layer Parameterizations Relative to Large Eddy Simulations, *Boundary-Layer Meteorology*, **79**, 1996, 131-175.

[2] Caretto, L.S., Gosman, A.D. and Patankar, S.V., Two Calculation Procedures for Steady, Three-Dimensional Flows with Recirculation, *3rd Int. Conf. on Numerical Methods in Fluid Mechanics, Lecture Notes in Physics*, **19**, 1972, 60-68.

[3] Conzemius, J.R. and Fedorovich, E., Dynamics of Shear Convective Boundary Layer Entrainment, *J. Atmospheric Sci.*, **66**, 2006, 1151–1178.

[4] Kirkpatrick, M.P., Ackerman, A.S., Stevens, D.E., and Mansour, N.N., On the Application of the Dynamic Smagorinsky Model to Large-Eddy Simulations of the Cloud-Topped Atmospheric Boundary Layer, *J. Atmospheric Sci.*, **63**, 2006, 526-546.

[5] Smyth, W.D. and Winters K.B., Turbulence and Mixing in Holmboe Waves, *J. Phys. Oceanogr.*, **33**, 2003, 694-711.

[6] Stevens, B., Moeng, C.H., Ackerman, A.S., Bretherton, C.S., Chlond, A., de Roode, S., and Zhu, P., Evaluation of Large-Eddy Simulations via Observations of Nocturnal Marine Stratocumulus, *Monthly Weather Review*, **133**, 2005, 1443-1462.

[7] Stewart, N.J., Holmes, D.W., Lin, W., Armfield, S.W., and Kirkpatrick, M.P., Direct Numeric Simulation of Sheared Convective Boundary Layer Entrainment with GPUs, *Proc. 5th Asia Pacific Congress on Computational Mechanics*, Singapore, 2013.